Available online at www.sciencedirect.com

SciVerse ScienceDirect

Scripta Materialia 68 (2013) 849–852

Scripta MATERIALIA

www.elsevier.com/locate/scriptamat

Room temperature creep behavior of free-standing Cu films with bimodal grain size distribution

N.N. Guo, J.Y. Zhang, P.M. Cheng, G. Liu* and J. Sun*

State Key Laboratory for Mechanical Behavior of Materials, Xi'an Jiaotong University, Xi'an 710049, People's Republic of China

Received 24 January 2013; accepted 3 February 2013
Available online 13 February 2013

The creep behavior of free-standing Cu films with bimodal grain size distribution was investigated at room temperature. It is found that the higher loading rate, the greater the primary creep strain rate and the smaller the steady-state creep strain rate. This unique creep behavior was explained by considering the competition between dislocation activities and dislocation stress fields. Given the grain size distribution, a modified phase-mixture model is proposed to predict the scaling behavior of creep rate and applied stress.

Keywords: Free-standing Cu films; Creep behavior; Grain size effect; Phase mixture model

Nanocrystalline (NC) metals with superstrength represent one class of promising structural materials but often suffer from low ductility [1–4]. Concomitantly, some newer strategies [5–10] have been tried out to overcome the Achilles' heel of NC materials, namely low ductility, among which manipulation of microstructural features in materials with bimodal *d*-distribution is a promising approach to dealing with Valiev's "paradoxon" [7]. For the materials (Cu) with micron-sized grains embedded inside a NC matrix, the matrix grains retain high strength (~350 MPa), while the bimodal distribution microstructure induces strain-hardening mechanisms that contribute to the extraordinary tensile ductility (~30% uniform elongation) [7].

Although the optimization of strength and ductility in NC metals embedded with larger grains ($d > 100$ nm) has led to new possibilities for mechanically improved structural materials, the benefits of NC materials are offset by the increased strain-rate sensitivity and increased creep rates compared to materials with greater grain size [1]. The plastic deformation of NC metals is severely influenced by the strain rate due to competing mechanisms of dislocation plasticity at higher strain rates and creep mechanisms at lower strain rates [3,10,11]. These unique behaviors are different from those for coarse-grained metals since grain boundaries (GBs) play an important role in dislocation activities at the nanoscale [12,13]. However, the loading/strain-rate effect on rate-controlled and time-dependent behavior, e.g. creep, of metals with bimodal microstructure is still unclear, in particular at room temperature.

On the other hand, the mechanical properties of thin films are often experimentally tested and theoretically analyzed on a substrate [14–17]. The constraint imposed by strong bonding between film and substrate implies that no sliding can occur at the film–substrate interface [18,19]. An additional constraint is that material transport may not proceed in the substrate, and diffusion therefore stops at the film–substrate interface [15]. To separate intrinsic thin-film properties from substrate contributions, experimental and analytical studies on free-standing thin films are of great importance. In this paper, we report that in free-standing Cu films with bimodal grain size distribution, faster loading rates result in greater primary creep strain rates and smaller steady-state creep rates at room temperature. The scaling behavior of steady-state creep rate with applied stress is quantitatively predicted by a modified phase-mixture model.

Ten micrometers thick Cu films with bimodal grain size distribution (~40 and ~220 nm) were produced on stainless steel substrate by an electrodeposition technique from an electrolyte of tartrate composed of $KNaC_2H_4O$, $CuSO_4$, $ZnSO_4$, NaOH at pH 12.4 and a temperature of 40 °C. The stainless steel was electropo-

* Corresponding authors. Tel.: +86 (0) 2982668695; fax: +86 (0) 2982663453 (J. Sun); e-mail addresses: lgsammer@mail.xjtu.edu.cn; junsun@mail.xjtu.edu.cn

1359-6462/$ - see front matter © 2013 Acta Materialia Inc. Published by Elsevier Ltd. All rights reserved.
http://dx.doi.org/10.1016/j.scriptamat.2013.02.008

lished by an electrolyte of 50% ethyl alcohol and 50% phosphoric acid under a direct current density of 15 A dm^{-2} before the electrodeposition. The pulse parameter for electrodeposition was t_{on}:t = 600 μs:60000 μs, and the current density was 0.375 A dm^{-2} with a magnetic stirring in order to obtain high-purity Cu films. After deposition, the film could be easily peeled from the substrate to yield free-standing Cu films with no evidence of damage introduced by the removal process, as verified by the scanning electron microscope observations. Free-standing Cu films were then electrodischarge machined (EDM) into dog-bone-shaped tensile samples with a gage length of 20 mm and width of 3 mm. At room temperature, uniaxial tensile testing was performed using a Micro-Force Test System (MTS® Tytron 250) at constant loading rates spanning from 0.5 to 50 mN s^{-1}. The creep tests were then performed under a load-control condition (covering a range from 100 to 230 MPa). Force–displacement data were automatedly recorded by the system.

The X-ray diffraction pattern of the free-standing Cu films reveals a strong ⟨1 1 1⟩ peak followed by a weak ⟨2 0 0⟩ peak, indicative of random in-plane orientations. Transmission electron microscopy (TEM) observations showed the Cu films to have a broad *d*-distribution spanning from 20 to 260 nm (see Fig. 1). A statistical analysis of about 600 grains indicated that free-standing Cu films exhibit two peaks (i.e. bimodal distribution) of grain volume fraction at average sizes of 100 and 220 nm, respectively, as displayed in Figure 1c. It should be noted that at such small grain sizes, almost no dislocation sources are contained within the grain interior. Dislocations are emitted from the GBs much more readily at the submicron and nanoscale, run across the grain interior and are absorbed by opposite GBs [12,13].

Figure 2a shows the creep strain (rate) as a function of time for a selected loading rate ~50 mN s^{-1} and at a stress level $\sigma \approx 200$ MPa in the holding regime. It appears that the creep strain rate (left Y-axis) sharply reduces and enters the steady creep stage while the creep strain (right Y-axis) monotonically increases with increasing time. Figure 2b demonstrates that the steady-state creep strain rate ($\dot{\varepsilon}_{SC}$) is a strong function of loading rate at different stress levels. It is found that the $\dot{\varepsilon}_{SC}$ monotonically increases with increasing stress level, similar to that of Au films [19]. (The primary creep strain rate $\dot{\varepsilon}_{PC}$, at the initial moment of the holding stage, behaves the same way.) Interestingly, in sharp contrast with $\dot{\varepsilon}_{PC}$, $\dot{\varepsilon}_{SC}$ monotonically increases with reducing loading rate (see Fig. 2c). In other words, the lower the loading rate, the greater $\dot{\varepsilon}_{SC}$, contrary to $\dot{\varepsilon}_{PC}$. These findings can be rationalized by considering the two competing effects between the dislocation (nucleation and motion) activities and the intensity of dislocation stress field caused by accumulation of dislocations. The former is determined by the external stress, while the latter is determined by the competition between the accumulation of inserted/absorbed dislocations and the reduction in their stress field as a function of time, probably by diffusion, at least for non-screw dislocations [20,21].

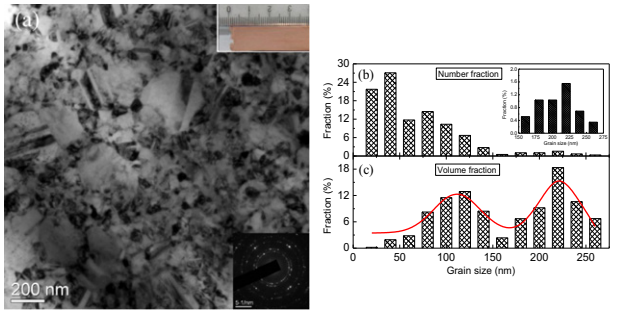

Figure 1. (a) Typical plan-view TEM image of free-standing Cu films. Bottom inset is the corresponding selected-area diffraction pattern (SADP) and upper inset is an optical image of the as-deposited free-standing Cu films peeled off from substrate; the statistical results of (b) number fraction and (c) corresponding volume fraction of grains at various sizes. Inset in (b) shows the statistical results for larger-sized grains.

As the sample is stretched faster to a constant stress level, more dislocations nucleated from the GBs are stored in the larger-sized grain interior instead of being absorbed by the opposite GBs [22] during the loading stage. During the primary creep stage, more dislocation pile-ups (and dislocations partly inserted in GBs) in larger grains would therefore lead to higher stresses on the leading dislocation, pushing it completely much more easily into the GB [20]. On the other hand, dislocation pile-ups or storage in GBs causes high repulsive stresses (fields) on the subsequent approaching dislocations and also influences dislocation nucleation and emission [20]. This in turn lowers the creep strain rate effectively. In this stage, however, the process of dislocation absorption significantly overwhelms the process of stress relaxation. As time elapses, more dislocations nucleate and accumulate at the GBs. This builds even higher stress fields instead of releasing stress concentrations, hindering the absorption of subsequent dislocations by GBs and finally reaching the steady-state creep stage. It is proposed that when these two dynamic processes balance, the creep strain rate eventually reaches a minimum and becomes near constant $\dot{\varepsilon}_{SC}$. Although individual dislocations dissolve in GBs in a few tens of seconds, even in a few minutes, their long-range stress field should remain large enough to repel other arriving dislocations [20,21]. In this regard, the higher stress fields (corresponding to faster loading rates) formed in the primary creep stage are more difficult to relax, which results in smaller $\dot{\varepsilon}_{SC}$.

In contrast, at slower loading rates more dislocations are absorbed by the GBs, creating higher stress fields/concentrations [20]. This is because slower loading rates provide sufficient time for the absorption of dislocations, leading to a much more severe stress field/concentration [22]. The heavier accumulation of dislocations, which generates higher repulsive stress, can effectively obstruct and eventually halt the processes of nucleation and emission of new dislocations from the GB. It results in a relatively lower creep strain rate during primary creep stage compared with the films that are loaded faster. In addition, the higher stress fields formed during the loading stage at a slower loading rate are likely to be relaxed faster than the ones formed at a faster loading rate. This is because fewer new dislocations are absorbed by GBs even with the assistance of external stress. With the passage of time, more dislocations are stored in the GBs, accompanied with the increased stress fields, which in turn obstructs, or even halts, the further

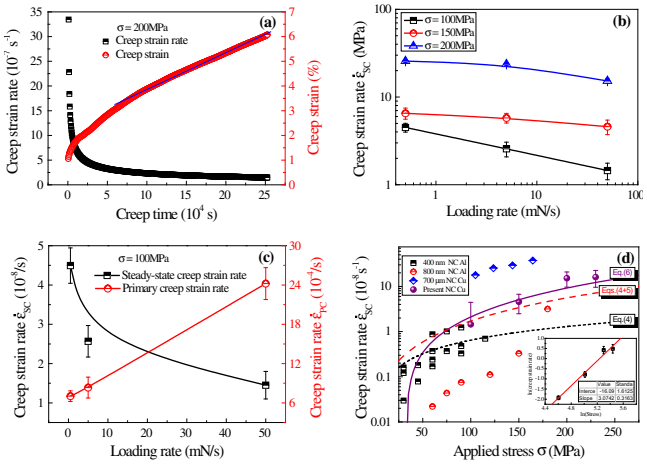

Figure 2. (a) The steady-state creep strain rate $\dot{\varepsilon}_{SC}$ (left axis) and creep strain (right axis) as a function of creep time. (b) The $\dot{\varepsilon}_{SC}$ as a function of loading rates at different stress levels. (c) The $\dot{\varepsilon}_{SC}$ (left axis) and primary creep strain rate $\dot{\varepsilon}_{PC}$ (right axis) as a function of loading rates. (d) A comparison of $\dot{\varepsilon}_{SC}$ for present Cu films with $d = 30$ nm NC Cu [28] and $d = 80$ nm NC Al films [11] as a function of stress at room temperature. The purple solid line, red dashed line and black short dashed line are calculated from Eq. (6), Eqs. 4 and 5, and Eq. (4), respectively. Inset in (d) showing the stress exponent $n \approx 3.07$ is obtained from the $\log(\dot{\varepsilon}_{SC}) - \log(\sigma)$ plot.

emission of dislocations during the primary creep stage [20,21]. Although the steady-state creep is finally achieved in a similar way to that described above, these processes can result in greater $\dot{\varepsilon}_{SC}$ in this stage. Thus, the loading history significantly affects $\dot{\varepsilon}_{PC}$ and $\dot{\varepsilon}_{SC}$ by changing the magnitude of the dislocation stress fields/concentrations. However, it should be pointed out that GB-mediated processes such as GB sliding and grain rotation and diffusion processes probably contribute to creep rate, since there is a high fraction of nanosized grains in the present free-standing films.

Figure 2d presents a typical $\dot{\varepsilon}_{SC} - \sigma$ curve of Cu films with bimodal grain size distribution at a loading rate of $\sim$50 mN s^{-1}, from which the stress exponent, n, is $\sim$3.07 can be determined based on the equation: $\dot{\varepsilon}_{SC} = C_1\sigma^n$, where C_1 is a constant (see the inset; at other loading rates $n \approx 3$ is also obtained). This value of $n \approx 3$ is much greater than the exponent predicted from the GB sliding mechanism $\sim$2 (see Eq. (5) below) [23] and from the diffusion creep mechanism $\sim$1 (see Eq. (4) below) [24] (i.e. Coble creep [25] and Nabarro–Herring creep [26,27]), as the dislocation mechanism contributes to the creep behavior of the present Cu films. In addition, the $\dot{\varepsilon}_{SC}$ monotonically increases with increasing stress, consistent with other reported $d = 30$ nm NC Cu [28] and $d = 80$ nm NC Al films [11]. Nevertheless, there is difference in the magnitude of room temperature $\dot{\varepsilon}_{SC}$ among the present Cu, NC Cu and NC Al. This is probably caused by the internal feature size and external thickness, loading rates, stacking fault energies, etc.

Following the spirit of Kim and Estrin [3], we employed their phase-mixture model which is able to provide a conclusive description of the deformation mechanism and mechanical properties of nanostructured materials, in order to fully understand the creep behavior of the present Cu films (for a review of the phase-mixture model, see Refs. [3,4] and references herein). The underlying concept in these "phase-mixture" models is that the grain interiors (GIs) are considered collectively as one phase, while the GBs are considered as a separate second phase. Here, we share the view that the GB diffusion and GB sliding "are closely connected and, perhaps, represent one and the same deformation mechanism" [3,4]. Furthermore, the stress in each of the two components (i.e., σ_{GB} for the GBs phase and σ_{GI} for the GI phase) of the "composite" is calculated based on the assumption that the strains in both phases are the same and are equal to the macroscopic strain ε [3,4]. The stress, determined by the rule-of-mixtures in the isostrain case, reads:

$$\sigma = f_{GB}\sigma_{GB} + f_{GI}\sigma_{GI} = \frac{3d^2w - 3dw^2 + w^3}{d^3}\sigma_{GB} + \left(1 - \frac{w}{d}\right)^3\sigma_{GI}, \quad (1)$$

where w is the GB width. In addition, we assume that dislocations nucleate from GBs and propagate across grains before being absorbed at the opposite boundaries. Under such conditions, it is reasonable to assert that the dislocation density (ρ) contributing to deformation will scale with the number of nucleation sites (M_S) per unit GB area A [24], which is strongly dependent on the external stress, and can be expressed as:

$$\rho = C_2M_S = C_3f(\sigma), \quad (2)$$

where C_2 and C_3 are constants, $f(\sigma) \propto \frac{1}{sm}\left(\frac{2\alpha\mu b}{d} + \frac{\gamma}{b}\right)$ is the partial dislocation nucleation stress dependence for the present grain size range ($\sim$20–260 nm) [12,13] which incorporates any possible stress dependence of M_S, and s is the Schmid slip factor, m is stress concentration factor ($\sim$2–4), μ is the shear modulus, γ is the stacking fault energy, the parameter α is of the order of unity and reflects the character of the dislocation and contains the scaling factor between the radius of curvature of the dislocation and grain size, and b is the magnitude of the Burgers vectors of the Shockley partial dislocation. Therefore, the contribution of dislocation glide to the creep rate of the GI phase ($\dot{\varepsilon}_{GI} = \dot{\varepsilon}_{Dis} + \dot{\varepsilon}_{Dif}$) can be examined in terms of the Orowan equation [29]:

$$\dot{\varepsilon}_{Dis} = \rho b\frac{L}{\delta}v_C = C_3f(\sigma)b\frac{L}{\delta}v_C = \frac{\beta b}{sm}\left(\frac{2\alpha\mu b}{d} + \frac{\gamma}{b}\right)\frac{\Omega\sigma_{GI}D_L}{l_dkT}, \quad (3)$$

where L is the dislocation glide distance, δ is the dislocation climb distance, D_L is the lattice diffusion coefficient, Ω is the atomic volume, k is the Boltzmann constant, T the absolute temperature, $l_d = (b/2\pi)\log(R/b)$, and R is the external radius of a cylindrical crystal containing a dislocation whose line lies along the cylinder axis.

In parallel, the diffusion-controlled mechanism for the GI phase is a combination of the Coble creep and the Nabarro–Herring creep mechanisms. Accordingly, the contributions of these two diffusion mechanisms to the creep strain rate for the GI phase can be written as [3]:

$$\dot{\varepsilon}_{Dif} = 14\pi\frac{\Omega\sigma_{GI}}{kT}\frac{w}{d}\frac{D_{GB}}{d^2} + 14\frac{\Omega\sigma_{GI}}{kT}\frac{D_L}{d^2}, \quad (4)$$

Where D_{GB} is the self-diffusion coefficient or GB diffusion and w is the GB width. Furthermore, the diffusion-controlled plastic flow of the GB phase was considered. The corresponding creep strain rate is given by [3,30]:

$$\dot{\varepsilon}_{GB} = \xi \frac{\Omega\sigma_{GB}}{kT}\frac{D_{GB}}{d^2} = 2\times 10^5 D_{GB}\frac{\mu b}{kT}\left(\frac{b}{d}\right)^3\left(\frac{\sigma_{GB}}{\mu}\right)^2, \quad (5)$$

where ξ is a numerical coefficient, and other symbols have the same meaning as above.

However, all the above equations are assumed to be the flow stress of the given grain (the smaller dimension/highest constraint determines the flow stress) and do not predict accurately the scaling behavior between $\dot{\varepsilon}_{SC}$ and stress in the present Cu films (see black dashed line and red short dashed lines in Figure 2d). In this case, the bimodal distribution of grain size must be considered, and hence the creep rate (and flow stress) distribution must be taken into account. Consequently, the overall creep rate $\bar{\dot{\varepsilon}}$ (and overall flow stress $\bar{\sigma}$) for each sample should be obtained by averaging and weighting the contribution of each grain (d_i) by its volume (f_i), which can be written as:

$$\begin{aligned}\bar{\dot{\varepsilon}} &= \sum_{i=1}^{i=N}(f_{GB-i}\dot{\varepsilon}_{GB-i} + f_{GI-i}\dot{\varepsilon}_{GI-i})f_i \\ &= \sum_{i=1}^{i=N}\left(\frac{3d_i^2 w - 3d_i w^2 + w^3}{d_i^3}\dot{\varepsilon}_{GB-i} + \left(1-\frac{w}{d_i}\right)^3\dot{\varepsilon}_{GI-i}\right)f_i,\end{aligned} \quad (6)$$

where $N \approx 13$ is the number of grains in the grain size distribution (see Fig. 1b), and $\dot{\varepsilon}_{GI-i}$ and $\dot{\varepsilon}_{GB-i}$ can be given by:

$$\begin{aligned}\dot{\varepsilon}_{GI\text{-}i} = \frac{\beta b}{sm}\left(\frac{2\alpha\mu b}{d_i}+\frac{\gamma}{b}\right)\frac{\Omega\sigma_{GI\text{-}i}D_L}{l_d kT} + 14\pi\frac{\Omega\sigma_{GI\text{-}i}}{kT}\frac{w}{d_i} \\ \times\frac{D_{GB}}{d_i^2} + 14\frac{\Omega\sigma_{GI\text{-}i}}{kT}\frac{D_L}{d_i^2},\end{aligned} \quad (7)$$

and

$$\dot{\varepsilon}_{GB-i} = \xi\frac{\Omega\sigma_{GB\text{-}i}}{kT}\frac{D_{GB}}{d_i^2}. \quad (8)$$

Taking a series of parameters: $s = 0.27$–0.47, $m = 2$–4, $b = 1.47\times10^{-10}$ m, $\alpha = 0.5$–1.5, $\mu = 48$ GPa, $\gamma = 41$ mJ m^{-2}, $\Omega = 1.18\times10^{-29}$ m^3, $D_L = 2.6\times10^{-20}$ m^2 s^{-1}, $l_d = b/2\pi = 2.34\times10^{-11}$ m, $k = 1.38\times10^{-23}$ J K^{-1}, $T = 298$ K, $w = 2b$–$5b$, $D_{GB} = 1.38\times10^{-23}$ m^2 s^{-1}, as seen in Figure 2d, consideration of the grain size contribution leads to a more reasonable scaling behavior of the steady-state creep rate $\dot{\varepsilon}_{SC}$ with applied stress σ for the present Cu films with bimodal d-distribution.

In summary, the loading history can significantly affect the unique creep behavior of free-standing Cu films with bimodal grain size distribution at room temperature, and the dislocation activities play an important role in the creep strain rate. The modified phase-mixture model can explain well the combination effects of grain size and stress on the creep behavior of metallic thin films with a broad grain size distribution.

This work was supported by the National Natural Science Foundation of China (Grant Nos. 50971097, 51201123), the 973 Program of China (Grant No. 2010CB631003), and the 111 Project of China (B06025). G.L. thanks the Fundamental Research Funds for the Central Universities and Tengfei Scholar project for support. J.Y.Z. thanks the China Postdoctoral Science Foundation funded Project for partial financial support (2012M521765).

[1] M.A. Meyers, A. Mishra, D.J. Benson, Prog. Mater. Sci. 51 (2006) 427.
[2] R.Z. Valiev, I.V. Alexandrov, Y.T. Zhu, T.C. Lowe, J. Mater. Res. 17 (2002) 5.
[3] H.S. Kim, Y. Estrin, Acta Mater. 53 (2005) 765.
[4] H.S. Kim, Y. Estrin, M.B. Bush, Acta Mater. 48 (2000) 493.
[5] E. Ma, JOM 58 (2006) 49.
[6] L. Lu, X. Chen, X. Huang, K. Lu, Science 323 (2009) 607.
[7] Y. Wang, M. Chen, F. Zhou, E. Ma, Nature 419 (2002) 912.
[8] J.Y. Kim, D.C. Jang, J.R. Greer, Adv. Funct. Mater. 21 (2011) 4550.
[9] J.Y. Zhang, X. Zhang, R.H. Wang, S.Y. Lei, P. Zhang, J.J. Niu, G. Liu, G.J. Zhang, J. Sun, Acta Mater. 59 (2011) 7368.
[10] N.J. Karanjgaokar, C.S. Oh, J. Lambros, I. Chasiotis, Acta Mater. 60 (2012) 5352.
[11] H. Hirakata, N. Fukuhara, S. Ajioka, A. Yonezu, M. Sakihara, K. Minoshima, Acta Mater. 60 (2012) 4438.
[12] J.Y. Zhang, P. Zhang, R.H. Wang, G. Liu, G.J. Zhang, J. Sun, Phys. Rev. B 86 (2012) 064110.
[13] J.-Y. Zhang, G. Liu, R.H. Wang, J. Li, J. Sun, E. Ma, Phys. Rev. B 81 (2010) 172104.
[14] R. Saha, W.D. Nix, Acta Mater. 50 (2002) 23.
[15] D. Weiss, H. Gao, E. Arzt, Acta Mater. 49 (2001) 2395.
[16] P.A. Gruber, J. Böhm, F. Onuseit, A. Wanner, R. Spolenak, E. Arzt, Acta Mater. 56 (2008) 2318.
[17] J. Zhang, J.Y. Zhang, G. Liu, Y. Zhao, X.D. Ding, G.P. Zhang, J. Sun, Scripta Mater. 60 (2009) 228.
[18] Z. Li, Y. Li, C. Zhang, J. Sun, Acta Mater. 60 (2012) 3057.
[19] N. Karanjgaokar, F. Stump, P. Geubelle, I. Chasiotis, Scripta Mater. 68 (2013) 551.
[20] F. Mompiou, D. Caillard, M. Legros, H. Mughrabi, Acta Mater. 60 (2012) 3402.
[21] J. Rajagopalan, C. Rentenberger, H. Peter Karnthaler, G. Dehm, M.T.A. Saif, Acta Mater. 58 (2010) 4772.
[22] C.E. Carlton, P.J. Ferreira, Acta Mater. 55 (2007) 3749.
[23] T.G. Langdon, J. Mater. Sci. 41 (2006) 597.
[24] A.H. Chokshi, Scripta Mater. 61 (2009) 96.
[25] R.L. Coble, J. Appl. Phys. 34 (1963) 1679.
[26] F.R.N. Nabarro, Philos. Mag. 16 (1967) 231.
[27] C. Herring, J. Appl. Phys. 21 (1950) 437.
[28] B. Cai, Q.P. Kong, L. Lu, K. Lu, Scripta Mater. 41 (1999) 755.
[29] T.H. Courtney, Mechanical Behavior of Materials, Waveland Press, Long Grove, 2000.
[30] Z.H. Cao, L. Wang, K. Hu, Y.L. Huang, X.K. Meng, Acta Mater. 60 (2012) 6742.